Chapter 4

Exploring the neuroprotective role of DHEA in inflammation*

Introduction

Docosahexaenoic acid (DHA, 22:6 n-3, **1**) is an omega-3 fatty acid which is essential for brain development and function (Figure 1).[1–4] DHA and its metabolites are abundant in the brain, representing 13-14% of total fatty acids in the cerebral cortex of primates.[5] One of the DHA metabolites is *N*-docosahexaenoylethanolamine (DHEA, **2**). DHEA is structurally related to the neurotransmitter anandamide (AEA) and is sometimes referred to as 'synaptamide', because it has been identified as a signaling lipid with potent neurotrophic and neuroprotective effects.[6,7] Inhibition of fatty acid amide hydrolase (FAAH), the main metabolic enzyme of DHEA, enhances some of the beneficial effects of DHA, which suggests that DHEA is involved in the physiological effects of DHA.[8,9] Despite their structural similarity, DHEA is much less active on the receptors of AEA, cannabinoid receptors type 1 and 2 (CB1R, CB2R). Instead, its neuronal effects are reported to be due to activation of GPR110.[10]

*The data presented in this chapter was gathered in collaboration with Andrea Martella, Eva van Rooden, Kim Wals, Hans den Dulk, Thomas Bakkum, Tom van der Wel, Herman S. Overkleeft, Sander van Kasteren, Mario van der Stelt.

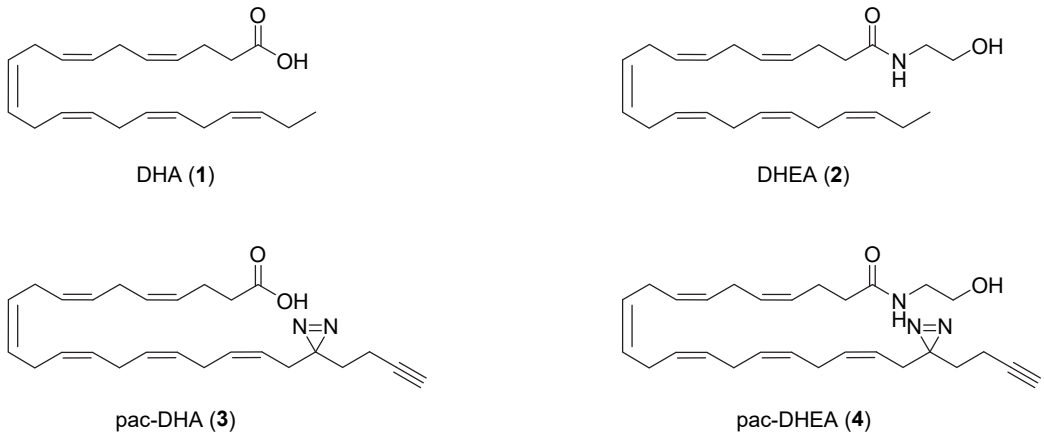

Figure 1 | DHA (**1**), DHEA (**2**) and their probe counterparts, photoaffinity-click (pac)-DHA (**3**) and pac-DHEA (**4**).

In addition to its role in neuronal growth, DHEA exerts neuroprotective effects by inhibiting the inflammatory response by immune cells in the central nervous system (CNS).[6,11] Although inflammation is a beneficial process to combat pathogens, persistent inflammation in the CNS is detrimental to neurons due to excessive production of pro-inflammatory cytokines and reactive oxygen and nitrogen species.[12] Chronic neuroinflammation is associated with many neurodegenerative diseases, such as multiple sclerosis (MS), Alzheimer's disease (AD) and Parkinson's disease (PD).[12–14] The inflammatory response in the CNS is regulated by microglia, which are a resident population of macrophage-like immune cells.[15,16] Microglia also modulate neuronal activity by releasing neurotrophic factors and removing immature synapses and excess neural precursor cells.[17,18] The pleiotropic effects of DHEA in the CNS indicate that it contributes to neuronal health through multiple pathways.

Activation of GPR110 by DHEA provides an anti-inflammatory signal.[19] Moreover, DHEA reduces COX-2-mediated production of pro-inflammatory eicosanoids in macrophages.[20] It is suggested that DHEA acts as a competitive or non-competitive inhibitor of COX-2, but it was also found to serve as a substrate of this enzyme, yielding oxidized metabolites.[21] This adds another level of complexity, as oxidative metabolism of DHEA introduces crosstalk between the epoxyeicosanoid and endocannabinoid signaling pathways.[22] Epoxyeicosanoids are synthesized from arachidonic acid by cytochrome P450 enzymes (CYP450) and have potent vasodilatory and anti-inflammatory effects.[23,24] DHEA can also serve as CYP450 substrate and the resulting metabolites act as cannabinoid receptor 2 (CB2R) agonists producing anti-inflammatory effects.[22] Another class of oxidized metabolites of DHEA, produced by lipoxygenase enzymes, are also potent agonists of the CB2R, which have organ-protective effects in an inflammatory model.[25] Finally, DHEA has been found to have additional cannabinoid receptor-independent anti-inflammatory effects.[20,26]

To further study the anti-inflammatory effects of DHEA and its metabolites, photoaffinity-based protein profiling (AfBPP) can be used to uncover protein interaction partners.[27] This approach, introduced in Chapter 3, uses bifunctional probes which consist of a ligand of interest modified with a photoreactive group and a bioorthogonal ligation handle. This combination allows for the discovery of probe-interacting proteins by sodium dodecyl sulfate polyacrylamide gel electrophoresis (SDS-PAGE) and fluorescence scanning, or alternatively, liquid chromatography-mass spectrometry (LC-MS, Figure 2).[28] Building on the methods and photoaffinity-click (pac)-DHA (**3**) developed in Chapter 3, the synthesis and application of photoaffinity probe pac-DHEA (**4**) is described in order to investigate the role of DHEA in neuroinflammation (Figure 1). This probe is used to map the lipid-protein interaction partners of DHEA in microglia using comparative AfBPP, which resulted in the discovery of novel protein interaction partners of DHEA. The role of these proteins in microglia was further investigated, which indicated that they may contribute to the anti-inflammatory effects of DHEA.

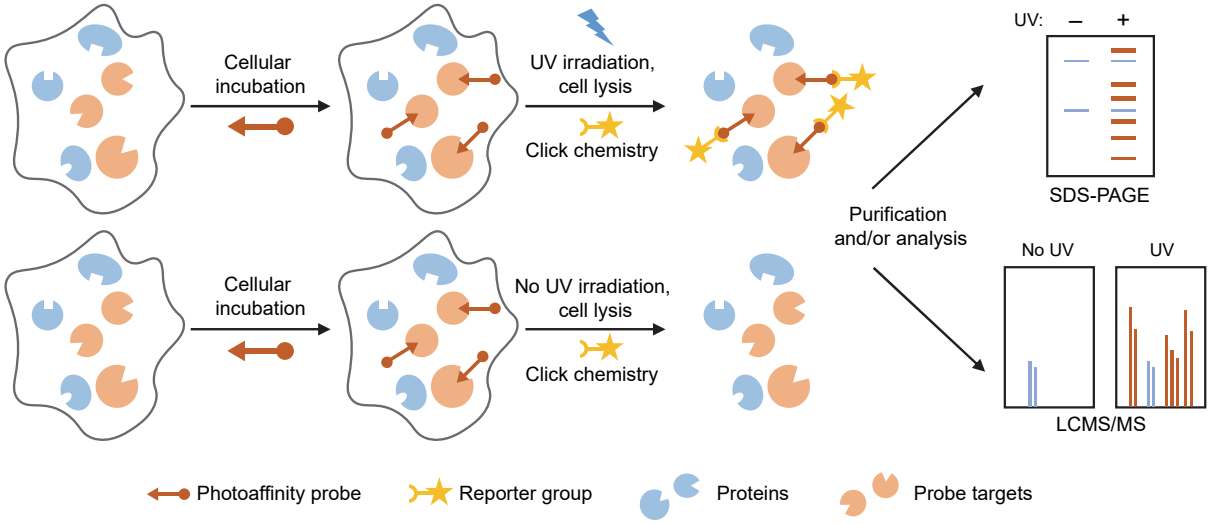

Figure 2 | Schematic overview of AfBPP experiment. Cells are incubated with a photoaffinity probe before UV irradiation or exposure to ambient light, followed by cell lysis and ligation of the probe-bound proteins to a fluorophore-azide or biotin-azide for SDS-PAGE or LC-MS/MS analysis respectively.

Results

Characterization of DHEA and pac-DHEA (**4**) in N9 microglia

To study the protein interaction partners of DHEA, pac-DHEA (**4**) was synthesized by condensation of pac-DHA (**3**) with ethanolamine (Figure 1). With both probes **3** and **4** in hand, it was investigated whether they showed similar anti-inflammatory properties as their parent lipids in lipopolysaccharide (LPS)-stimulated N9 microglia cells, which are widely used as an *in vitro* model of neuroinflammation.[29] The cells were incubated with DHA, DHEA, probe **3** or **4** at 10 µM for 4 h before addition of 25 ng/mL LPS. The effect of the lipids on a number of pro-inflammatory gene transcripts (*IL6, Ptgs2, Tlr2* and *CD86*) was quantified by qPCR (Figure 3). DHEA and pac-DHEA (**4**) were equipotent in their reduction of *IL6, Ptgs2, Tlr2* and *CD86* mRNA levels, which indicated that the photoaffinity probe retained the anti-inflammatory properties of DHEA. In line with previous reports, it was found that DHEA was more effective than DHA in suppressing the LPS-induced expression of pro-inflammatory genes, except of *Ptgs2*.[11,30] This result indicates that DHEA and DHA exert different biological activities and suggests that they have different interaction partners.

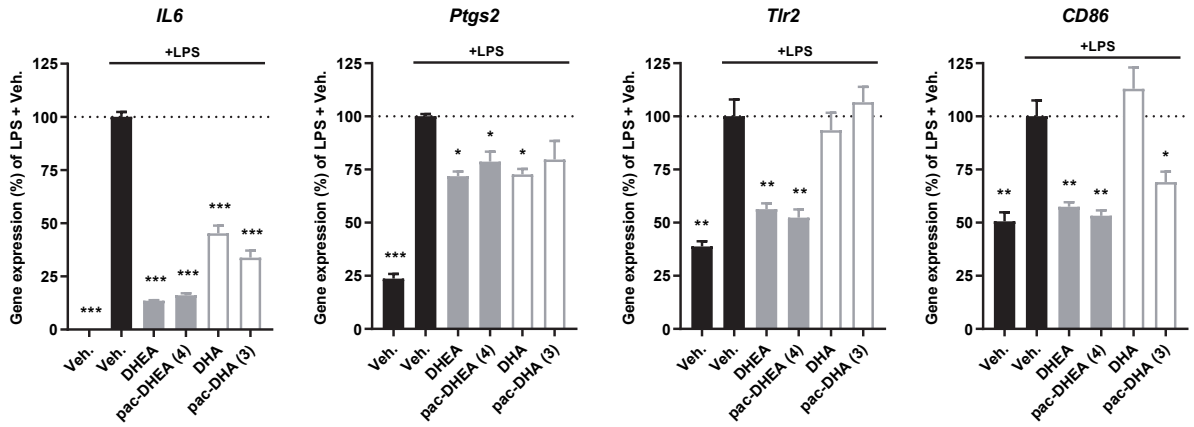

Figure 3 | Effect of lipids on inflammatory markers of N9 microglia. N9 microglia were pretreated with indicated lipid (10 µM) or vehicle for 4 h before LPS stimulation (25 ng/mL) for 24 h. Values reported are mRNA expression of inflammation-related genes as measured by qPCR and normalized to LPS-treated vehicle control. Data represent means ± SEM (n = 2). * p <0.05, ** p <0.01, *** p <0.001 in comparison to LPS-treated control (dotted line) using a one-way ANOVA with Dunnett's multiple comparisons correction.

Photoaffinity labeling reveals pac-DHEA-interacting proteins

To discover DHEA-interacting proteins, the photoaffinity probes were used in an AfBPP experiment using N9 microglia. To capture the probe-interacting proteins, N9 microglia were treated with pac-DHA (**3**) or pac-DHEA (**4**) (10 µM) and incubated for 24 h to simulate the qPCR experiments. After incubation, supernatant was removed and the cells were washed with PBS followed by irradiation (350 nm, 10 min, "UV") or exposure to ambient light ("no UV"). Cells were lysed and the probe-labeled proteins were conjugated to Cy5-N_3 under copper(I)-catalyzed azide-alkyne cycloaddition (CuAAC) conditions. Separation of the labeled proteins by SDS-PAGE and in-gel fluorescence scanning demonstrated UV-dependent labeling of proteins by probe **4** (Figure 4A).

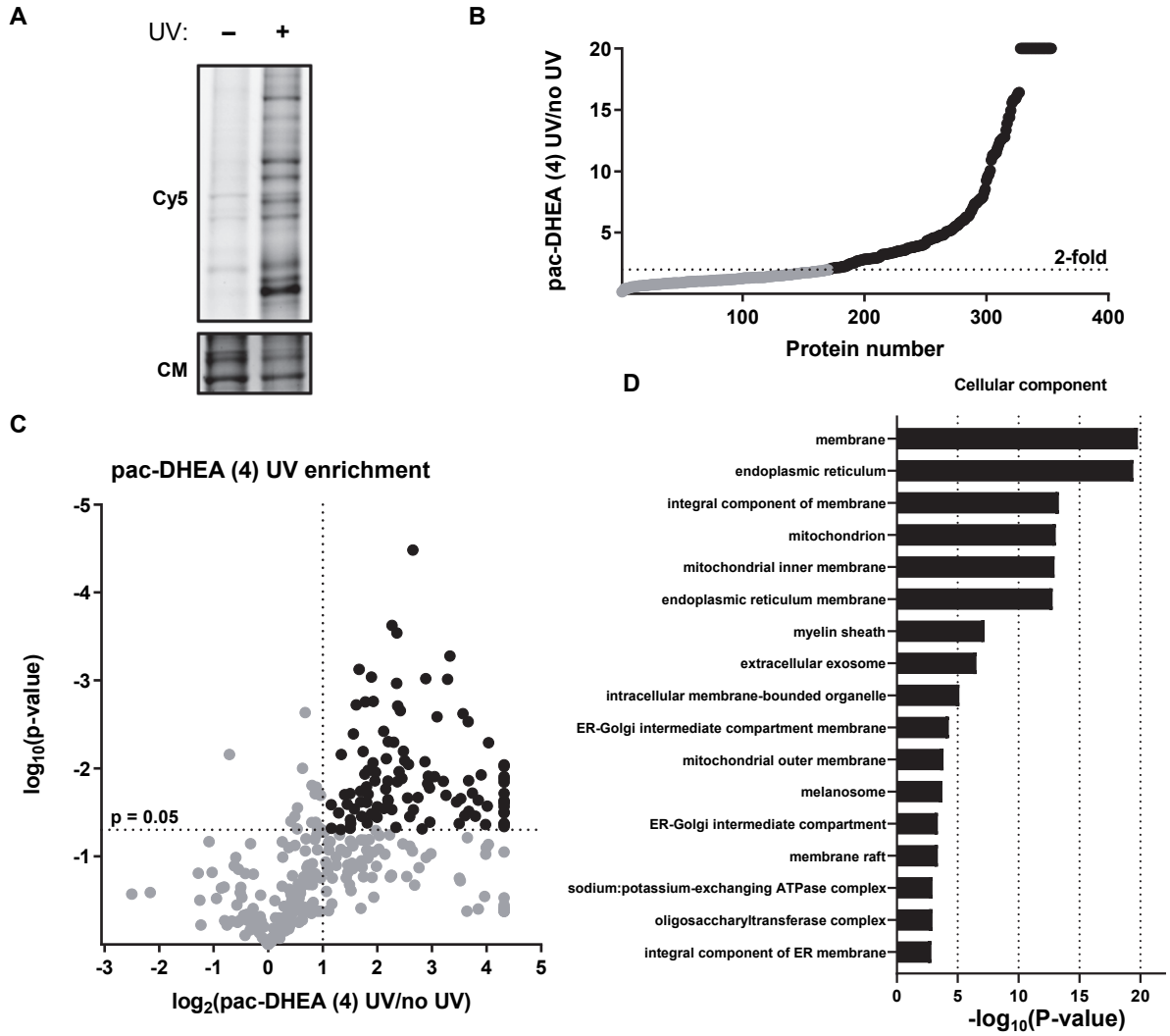

Figure 4 | Pac-DHEA (4)-interacting proteins in N9 microglia. (A) Gel-based AfBPP analysis of pac-DHEA (**4**)-interacting proteins in N9 microglia. **(B)** Waterfall plot of proteins identified in pulldown experiment with 10 µM pac-DHEA (**4**). UV enrichment was capped at 20-fold and proteins with a ratio >2 are highlighted in black. **(C)** Volcano plot of proteins identified in pulldown experiment with 10 µM pac-DHEA (**4**). UV enrichment was capped at 20-fold and proteins with a ratio >2 and p-value <0.05 are highlighted in black. **(D)** GO enrichment analysis of significantly UV-enriched pac-DHEA (**4**) targets.

To identify these targets, probe-bound proteins were ligated to biotin-N_3, enriched using avidin-coated agarose beads, digested by trypsin and analyzed by LC-MS/MS.[31] Proteomic analysis resulted in 353 identified proteins with at least 2 unique peptides (Figure 4B). Out of these, 105 were designated as pac-DHEA (**4**)-interacting targets using >2-fold UV enrichment and a p-value <0.05 as cutoff criteria (Figure 4C). GO enrichment analysis of the cellular component annotation of these targets showed that mainly membrane proteins and proteins associated with the endoplasmic reticulum (ER) and mitochondria were enriched (Figure 4D).[32,33]

To distinguish between lipophilic, nonspecifically-interacting proteins and genuine probe targets, the probe **4**-interacting proteins were compared to the proteins identified by pac-DHA (**3**). To this end, label-free quantification (LFQ) values of pac-DHEA (**4**) targets were plotted against that of pac-DHA (**3**), which revealed eleven targets specific for probe **4** (Figure 5A, B and Table S3). These targets consisted in part of known lipid-metabolizing proteins and known AEA interaction partners previously found by AEA-based probes.[34] Of these targets, three proteins with unknown function or mechanism of action were chosen for further investigation, neudesin (NENF), adipocyte plasma membrane-associated protein (APMAP) and glutathione S-transferase Mu 1 (GSTM1). To confirm GSTM1 among the GSTM family, the identified peptides were compared to the known sequences. Of the peptides found for GSTM1, two were unique for GSTM1 within the family (Figure 5C).

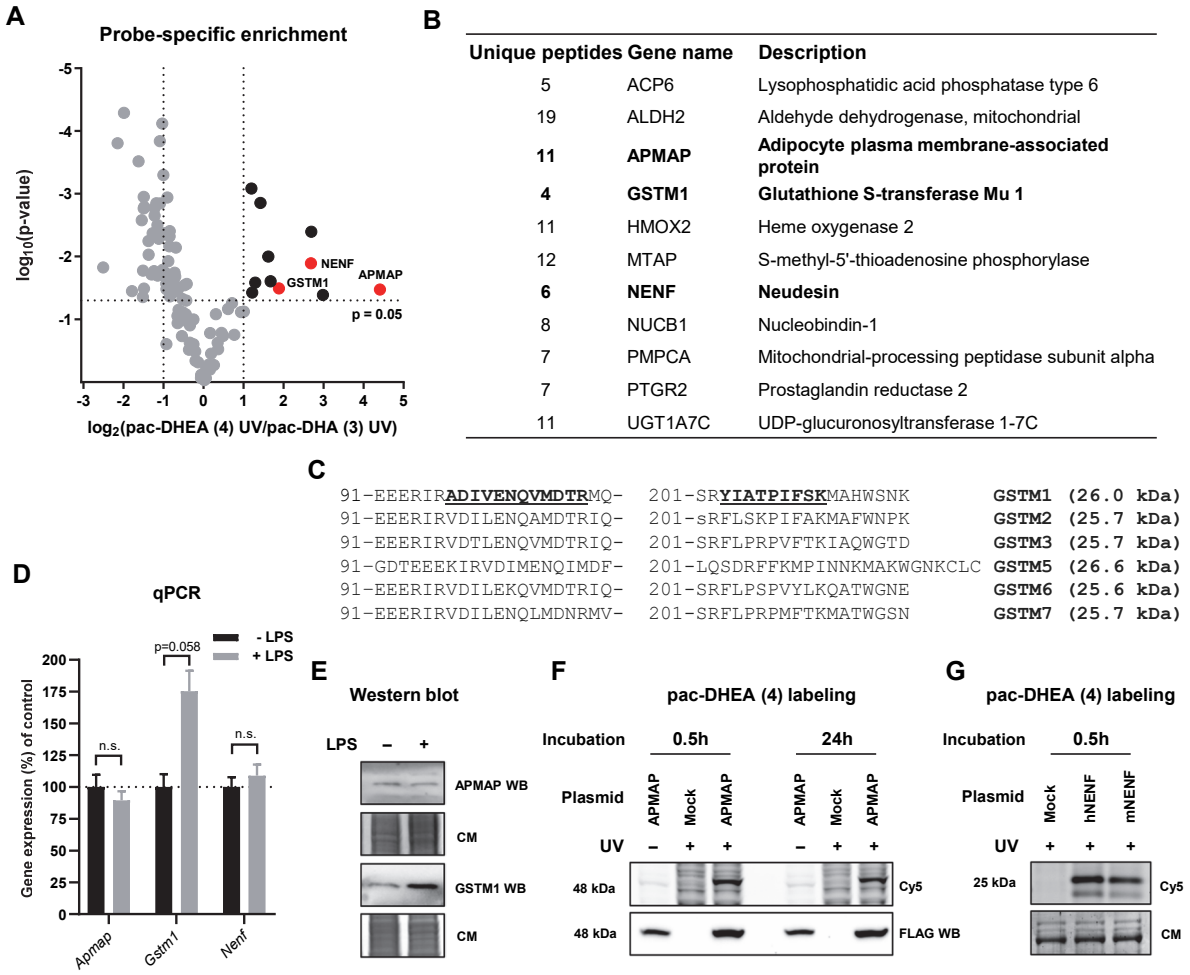

Unique peptides	Gene name	Description
5	ACP6	Lysophosphatidic acid phosphatase type 6
19	ALDH2	Aldehyde dehydrogenase, mitochondrial
11	**APMAP**	**Adipocyte plasma membrane-associated protein**
4	**GSTM1**	**Glutathione S-transferase Mu 1**
11	HMOX2	Heme oxygenase 2
12	MTAP	S-methyl-5'-thioadenosine phosphorylase
6	**NENF**	**Neudesin**
8	NUCB1	Nucleobindin-1
7	PMPCA	Mitochondrial-processing peptidase subunit alpha
7	PTGR2	Prostaglandin reductase 2
11	UGT1A7C	UDP-glucuronosyltransferase 1-7C

Figure 5 | Specifically enriched pac-DHEA (4) targets. (A) Volcano plot of LFQ values of pac-DHEA (**4**) versus pac-DHA (**3**) of probe **4** UV-enriched targets. Probe **4**-specific targets are in black, NENF, GSTM1 and APMAP are highlighted in red. **(B)** List of all probe **4**-specific targets. **(C)** Amino acid sequences for the GSTM family starting at amino acid 91 and 201 as per the mouse UNIPROT database with two identified peptides indicated in bold. **(D)** qPCR analysis of *Apmap*, *Gstm1* and *Nenf* genes in unstimulated or LPS-stimulated (25 ng/mL) N9 microglia. Data represent means ± SEM (n = 2). Student's t-tests were used to test for significance versus control. **(E)** Western blot of N9 microglia against APMAP and GSTM1 shows expression of both proteins and increased GSMT1 protein upon LPS stimulation (100 ng/mL). **(F)** Gel-based AfBPP with pac-DHEA (**4**) in APMAP-overexpressing HEK-293-T cells after 0.5 and 24 h probe incubation. **(G)** Gel-based AfBPP with pac-DHEA (**4**) on mouse or human NENF-expressing HEK-293-T supernatant. Coomassie served as a protein loading control.

The expression of NENF, APMAP and GSTM1 in N9 cells was further investigated by qPCR and western blot. *Apmap*, *Gstm1* and *Nenf* mRNA could be detected and APMAP and GSTM1 protein was detected by specific antibodies (Figure 5D/E). mRNA and protein levels of GSMT1 showed an increase upon LPS stimulation, which is consistent with its reported involvement in inflammatory signaling.[35] Next, the three proteins were overexpressed in HEK-293-T cells to confirm that they are targets of probe **4**. Gel-based AfBPP revealed that APMAP could be labeled by the probe after a short (0.5 h) or long (24 h) incubation time (Figure 5F). Probe labeling of NENF, an extracellular protein, was observed in the supernatant of NENF-overexpressing HEK-293-T cells (Figure 5G). GSTM1 was overexpressed in HEK-293-T cells, but could not be labeled at any incubation time. This indicated that APMAP and NENF, but not GSTM1, are direct protein targets of pac-DHEA (**4**).

Characterization of NENF, GSMT1 and APMAP in N9 microglia

The three proteins were further investigated for their role in inflammatory response by measuring secreted pro-inflammatory markers interleukin-6 (IL-6) and nitric oxide (NO). NO is rapidly oxidized in cells to form nitrite, which can be detected and quantified through its reactivity towards 2,3-diaminonaphthalene (DAN).[36,37] Incubation of N9 cells with LPS induced the formation of IL-6 as measured by ELISA and nitrite as measured using a DAN assay (Figure 6A, B, Figure S1, S2).[38] DHEA reduced both NO and IL-6 production in a dose-dependent manner (Figure 6A, B, Figure S2). In contrast to previously published results, which indicated that CYP450-derived epoxide metabolites of DHEA play a critical role in microglial inflammatory response,[22] the broad-spectrum CYP inhibitor ketoconazole and a soluble epoxide hydrolase inhibitor did not affect the anti-inflammatory effects of DHEA (Figure S3).

Next, the effect of the three proteins on LPS-induced inflammatory response by N9 cells was investigated. NENF acts as an extracellular signaling factor, and recombinant NENF has been shown to have neurotrophic effects on neuronal cells under serum-free conditions.[39] Therefore, N9 cells were incubated with or without fetal calf serum and supplemented with recombinant NENF protein or bovine serum albumin (BSA) as control. Under these conditions, NENF reduced LPS-induced NO production slightly in serum-free medium, but not in combination with DHEA (Figure 6C, D).

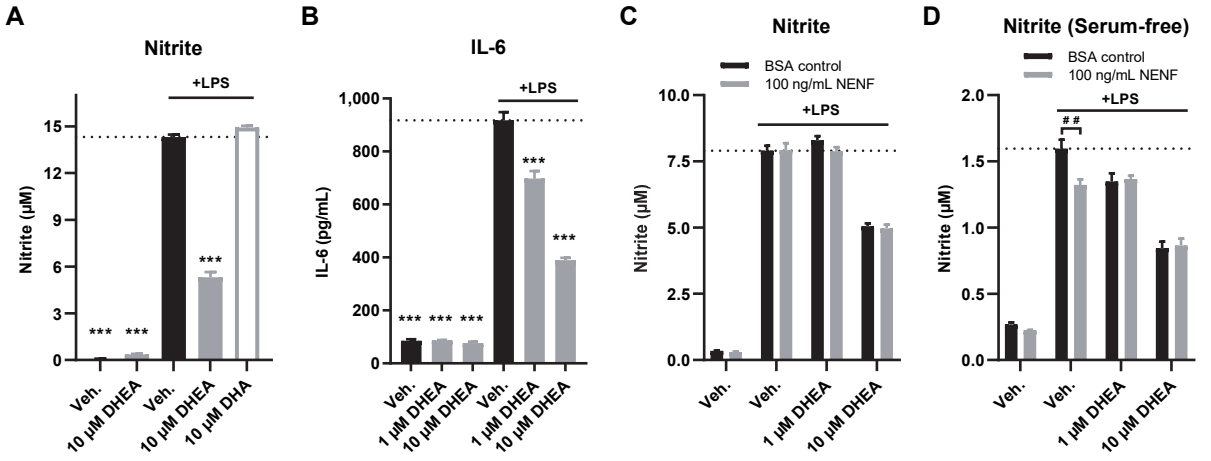

Figure 6 | Effect of DHA, DHEA and NENF on inflammatory markers. N9 microglia were pretreated with indicated lipid or vehicle for 4 h before LPS stimulation (100 ng/mL) for 24 h. Supernatant was collected for **(A, C, D)** DAN assay or **(B)** IL-6 ELISA and viability was tested by MTT assay (Figure S1). For the NENF treatment, N9 microglia were cultured in full medium or serum-free medium supplemented with 0.1% delipidated BSA for 3 h, after which they were treated with indicated combination of recombinant human NENF or BSA, and DHEA or vehicle for 4 h before LPS stimulation (100 ng/mL) in the corresponding medium. Data represent means ± SEM (n = 3-6). *** p <0.001 in comparison to LPS-treated control (dotted line) using a one-way ANOVA with Dunnett's multiple comparisons correction. ## p <0.01 using a one-way ANOVA between all conditions with Tukey's multiple comparisons correction.

Next, since GSTM1 and APMAP have no known function or inhibitors, the role of these proteins in inflammatory response was studied by overexpression in N9 cells. Since most traditional methods of introduction of foreign DNA in microglial cells result in cell death or premature activation, stable expressing N9 cells were made using lentiviral vectors.[40,41]

To follow incorporation of the genetic material during the selection procedure, GFP fusions of GSTM1 and APMAP were used. HEK-293-T cells were transfected to obtain lentiviral particles carrying vectors encoding GFP, GSMT1-GFP and APMAP-GFP, which were subsequently used to infect N9 microglia. Selection for cells which incorporated the DNA of interest afforded populations with good (>90% of cells) expression of GFP and acceptable (50-75% of cells) expression of GSTM1-GFP and APMAP-GFP based on fluorescent signal. Expression of GSTM1-GFP and APMAP-GFP was confirmed by western blot (Figure S4A, B) and localization was investigated by confocal microscopy of live cells (Figure S4C). This showed homogeneous localization of GFP and GSTM1-GFP throughout the cell, whereas APMAP-GFP showed exclusion from the nucleus, which was consistent with literature.[42]

Next, IL-6 and nitrite levels in LPS-stimulated GFP-, GSTM1-GFP- and APMAP-GFP-expressing cells were determined (Figure 7). Both GSTM1-GFP and APMAP-GFP overexpression did not elicit an immune response or affect cell viability (Figure S5), but upon LPS stimulation the NO and IL-6 response was strongly and significantly increased compared to control cells expressing GFP. The increased nitrite and IL-6 levels in both GSTM1-GFP- and APMAP-GFP-expressing cells were reduced by pretreatment with DHEA. Of note, DHA only partly reduced levels of IL-6, but not nitrite, in GSTM1-GFP- and APMAP-GFP-expressing cells.

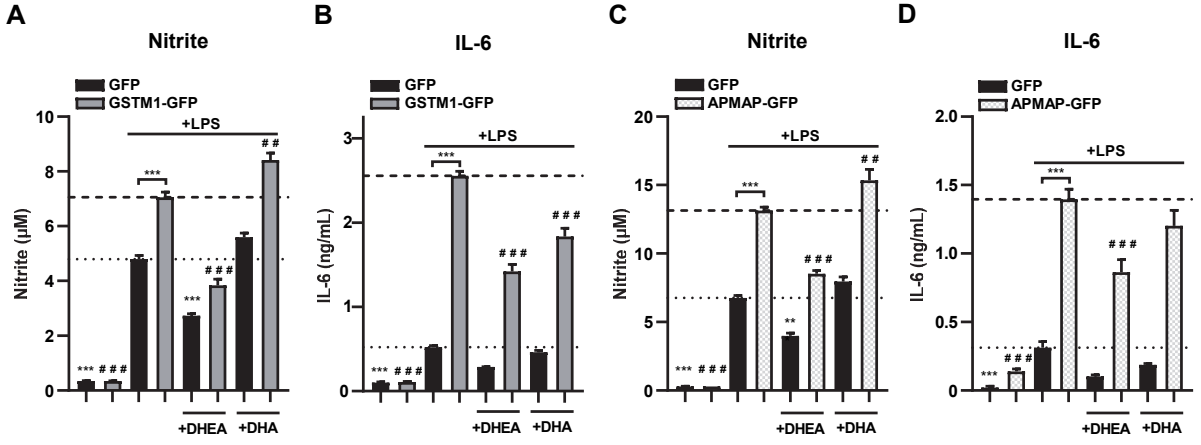

Figure 7 | Effect of expression of GFP, GSTM1-GFP or APMAP-GFP on inflammatory markers. (A,B) GSTM1-GFP-, **(C, D)** APMAP-GFP- or GFP-expressing N9 microglia were pretreated with indicated lipid or vehicle for 4 h before LPS stimulation (100 ng/mL) for 24 h. Supernatant was collected for DAN assay or IL-6 ELISA and viability was tested by MTT assay (Figure S5). Data represent means ± SEM (n = 4). *** p <0.001; ** p <0.01 in comparison to LPS-treated GFP-expressing cells (dotted line), ### p <0.001; ## p <0.01 in comparison to LPS-treated GSTM1-GFP- or APMAP-GFP-expressing cells (dashed line) using a one-way ANOVA between all conditions followed by Tukey's multiple comparisons correction.

Discussion and conclusion

DHEA is an omega-3 fatty acid derivative with pleiotropic effects in the brain. It is known to have a role in neurogenesis, neuritogenesis and synaptogenesis, but also to reduce the inflammatory response of immune cells. Although large improvements have been made to detect and quantify DHEA and its metabolites, this does not allow for the discovery of novel protein targets that bestow their anti-inflammatory properties. This is enabled by photoaffinity probes, which have been successfully used to characterize lipid-protein interactions of several lipid classes.[34,43–45] In this chapter, the role of DHEA in neuroinflammation was investigated by characterization of its anti-inflammatory effects in a microglial cell line and the protein interaction landscape was investigated using a DHEA-based photoaffinity probe. DHEA dose-dependently reduced inflammatory response to a greater extent than DHA. Inhibition of CYP450 and sEH enzymes did not alter this effect, indicating that epoxide metabolites of DHEA were not involved in LPS-stimulated N9 microglia. Photoaffinity probe **4** had the same anti-inflammatory capacity as its parent lipid, which indicated that the introduction of the minimalist bifunctional photoreactive linker with an alkyne ligation tag was tolerated. Probe **4** was used to identify 105 pac-DHEA-interacting proteins. Of these, 11 were deemed DHEA-specific after deselection, of which three were further investigated.

NENF is a 171 amino acid secreted protein expressed abundantly in the central nervous system and was identified as a heme-binding neurotrophic factor.[46–48] It signals for neuronal differentiation and survival through the mitogen-activated protein kinase (MAPK) and phosphatidylinositol 3-kinase (PI3K) pathways.[39,47] Specific receptors remain unknown.[49] Recombinant NENF did not alter NO production in complete medium upon LPS stimulation, however, the NO response was reduced by NENF when N9 microglia were cultured in serum-free medium. In line with previously reported neuroprotective properties of NENF[39] and interaction with AEA,[34] NENF could act as a facilitator for the intercellular exchange of signaling lipids like DHEA and AEA in the brain.

GSTM1 is part of a family of enzymes responsible for the metabolism of a broad range of xenobiotics and carcinogens.[50] GSTM1 was found to promote pro-inflammatory signaling in mice and to be required in astrocytes for the activation of nuclear factor κB and stimulated the formation of pro-inflammatory mediators.[35] Knockdown of GSMT1 in astrocytes resulted in attenuated activation of microglia in the prefrontal cortex of mice in response to LPS stimulation.[35] The results presented here show that GSTM1 is also present in microglia and its expression is increased upon LPS stimulation. Overexpression of GSTM1-GFP in N9 microglia exacerbated the inflammatory response to LPS. DHEA could partially reverse this effect, while DHA was less effective. Since probe **4** did not directly label recombinant GSMT1 in HEK-293-T cells, an oxidative metabolite of DHEA produced by lipoxygenases or cyclooxygenases may be responsible for the interaction with GSMT1. Previously, GSMT1 has been implicated in neuroinflammation[35] and its null polymorphism is associated with increased risk of

inflammatory disease[51] and cancer.[52,53] Based on the results reported in this study, it can be speculated that GSTM1 inactivates not only toxic metabolites, but also anti-inflammatory lipids, thereby exacerbating the inflammatory response.

APMAP was identified as an integral plasma membrane protein with a large extracellular C-terminal domain.[54] It induces differentiation of 3T3-L1 cells into adipocytes,[54] but it is also expressed in non-adipose tissues, like liver, central nervous system, blood vessels and on the cell surface of CD14+ monocytes and endothelial cells.[42] It has esterase activity and its sequence homology with paraoxonase family members indicates that it might be involved in detoxification processes.[42] Here, it was shown to interact with pac-DHEA and to increase the inflammatory response to LPS in N9 microglia, which could be partially prevented by DHEA. The interaction of APMAP with pac-DHEA (**4**) and its homology to paraoxonases suggests that it could be involved in metabolism of immunomodulatory lipids.

In conclusion, lipid photoaffinity probes can be used to investigate protein-lipid interactions that infer the anti-inflammatory properties of omega-3 fatty acids and metabolites. Control probes are needed to distinguish between specific and nonspecific interactions. Applying DHA- and DHEA-based photoaffinity probes provided an overview of the interaction landscape in microglial cells and provide a basis for further investigation of the role of these omega-3 fatty acids in neuroinflammation.

Experimental procedures

General

Lipids were purchased from Cayman Chemicals and stored as 10 mM ethanolic stocks under nitrogen at -80 °C. Inhibitors were purchased from Cayman Chemicals or Sigma Aldrich and stored as 10 mM DMSO stocks at -20 °C. LPS from *Escherichia coli* (O111:B4, Sigma Aldrich) was dissolved in PBS and stored at 200 µg/mL at -20 °C. Human recombinant NENF was obtained from R&D Systems (6714-ND-050), reconstituted to 100 µg/mL in PBS and stored at -80 °C. FP-TAMRA was purchased from Thermo Fisher. MB064 was synthesized in-house as previously described.[55] All other reagents were purchased from Sigma Aldrich or Cayman Chemicals unless otherwise specified.

Cloning

DNA oligos were purchased at Sigma Aldrich or Integrated DNA Technologies. Cloning reagents were from Thermo Fisher. Full-length cDNA encoding human NENF or murine APMAP, NENF and GSTM1 was obtained from Source Bioscience. Expression constructs were generated by PCR amplification and restriction/ligation cloning into a pcDNA3.1 vector, in frame with a C-terminal FLAG tag or, in case of GFP fusion constructs, a C-terminal GFP-FLAG tag. Lentiviral vectors (pLenti6.3/V5-DEST, pMD2.G, pRSV-Rev and pMDLg/pRRE) were kind gifts from Dr. Rolf Boot (Leiden University). Lentiviral expression constructs were generated by PCR amplification of the GFP, APMAP-GFP-FLAG or GSTM1-GFP-FLAG sequence and restriction/ligation cloning into a pLenti6.3/V5-DEST vector. All plasmids were isolated from transformed XL10-Gold or DH10B competent cells (prepared using *E. coli* transformation buffer set, Zymo Research) using plasmid isolation kits following the supplier's protocol (Qiagen). All sequences were verified by Sanger sequencing (Macrogen).

General cell culture

HEK-293-T cells were cultured at 37 °C under 7% CO_2 in DMEM (Sigma Aldrich, D6546) containing phenol red, stable glutamine, 10% (v/v) New Born Calf Serum (Thermo Fisher) and penicillin and streptomycin (200 µg/mL each, Duchefa). Cells were passaged twice a week at 80-90% confluence by resuspension in fresh medium.

N9 microglia were cultured at 37 °C under 5% CO_2 in RPMI 1640 (Sigma) containing phenol red, stable glutamine, 10% (v/v) sterile-filtered Fetal Calf Serum (Thermo Fisher) and penicillin and streptomycin (200 µg/mL each, Duchefa). Cells were passaged every two days by washing with PBS and trypsinization, subsequently quenching the trypsin with medium and removal of the trypsin by spinning down the cell suspension (200 *g*, 5 min). The resulting pellet was resuspended in culture medium by vortexing and subsequently seeded on new plates. Cells were tested regularly for mycoplasma contamination. Cultures were discarded after 2-3 months of use.

N9 lentivirus infection

To produce lentiviral particles, HEK-293-T cells were seeded on 10 cm dishes 24 h prior to transfection. Culture medium (DMEM) was then aspirated and replaced with 5 mL fresh medium. A 3:1 (m/m) mixture of PEI (30 µg/dish) and plasmid DNA (10 µg/dish, 1:1:2:4 ratio (m/m) of pMD2.G, pRSV-Rev, pMDLg/pRRE, and pLenti6.3/V5-DEST encoding GFP, GSMT1-GFP or APMAP-GFP) was prepared in serum-free culture medium (1 mL) and incubated for 15 min at rt. Transfection was performed by dropwise addition of the PEI/DNA mix to the cells. After 24 h, medium was replaced with fresh medium supplemented with HEPES pH 7.4 (20 mM final). After 24 h, the supernatant was collected in a 15 mL tube, spun down (10,000 *g*, 5 min) and filtered over a 0.45 µm sterile filter and used immediately.

For the infection, $1.0x10^5$ N9 cells were plated on 6-well plates 24 h prior to infection. The medium (RPMI) was aspirated and replaced with 1 mL fresh medium. This was supplemented with 1 mL of HEK-293-T supernatant containing the lentiviral particles and the cells were cultured for 24 h. The medium was removed and replaced with 4 mL culture medium (RPMI). After 24 h, the medium was replaced with 4 mL medium containing 2 µg/mL blasticidin S and the cells were maintained on 2 µg/mL blasticidin S for two weeks, splitting cells when confluent and replacing the medium at least every two days. For subsequent experiments, the cells were plated in medium without blasticidin S.

RNA extraction and cDNA synthesis

Cells were lysed in Invitrogen TRIzol reagent (Thermo Fisher) in a total volume of 500 µL and frozen at -80 °C. RNA extraction was performed following the supplier's protocol with minor modifications. In short, 100 µL $CHCl_3$ was added to the lysates and the sample was thoroughly vortexed and centrifuged (12,000 *g*, 15 min). The clear lysate was transferred to a new vial and isopropanol was added (1:1 v/v). This was vortexed, incubated for 10 min and centrifuged (7,500 *g*, 10 min). The RNA pellet was then washed twice with 750 µL of 75% ethanol and dried by evaporation. The pellet was resuspended in 10 µL of RNase free DEPC water (BioSphere) and the RNA concentration and purity were determined using a DeNovix DS-11 spectrophotometer. RNA with an A_{260}/A_{280}-ratio between 1.95 and 2.05 was considered to be of sufficient quality. The samples were brought to equal concentration by diluting with DEPC water. RNA was then mixed with dNTPs (0.5 mM) and oligodT (5 µM), and shortly heated up to 85 °C. Subsequently, RT-buffer (ThermoFisher), Reverse transcriptase (Thermo Fisher, EP0752) and RiboLock (2 units, Thermo Fisher, O0381) was added in a total volume of 10 µL and the cDNA was generated in 30 min at 50 °C in a thermal cycler.

Quantitative real-time polymerase chain reaction

Quantitative real-time polymerase chain reaction (qPCR) was performed with 10 ng of RNA as a template. Forward and reverse primers for the indicated gene were added both at 0.3 µM final concentration, with 7.5 µL of 2*SYBR Green Master mix (BioTools, B21202) in a total volume of 15 µL. Amplification was performed in a BioRad CFX96 Touch Real-time PCR. 5 min at 95 °C was done to heat-start the polymerase-activity. 40 cycles were then performed consisting of 15 seconds of denaturation at 95 °C, followed by 45 seconds of annealing and elongation at 60 °C. Afterwards, the melting temperature was measured to assess amplicon integrity by performing 60 cycles of 65 °C + 0.5 °C/cycle for 5 seconds/cycle. Used primers sets are listed in Table S1.

Table S1 | Primers used in qPCR experiments.

Gene	Forward primer	Reverse primer
Hprt	TTGACACTGGTAAAACAATGC	GCCTGTATCCAACACTTCG
Il6	TAGTCCTTCCTACCCCAATTTCC	TTGGTCCTTAGCCACTCCTTC
Ptgs2	TGAGCAACTATTCCAAACCAGC	GCACGTAGTCTTCGATCACTATC
Cd86	TGTTTCCGTGGAGACGCAAG	TTGAGCCTTTGTAAATGGGCA
Tlr2	AGGTGCGGACTGTTTCCTTC	AGATTTGACGCTTTGTCTGAGG
Apmap	GAGGTCAAGGAGGGCAGTTC	GGGTTCTTTGAAGCTGAAACTCT
Gstm1	TAATTGGGATTGGTGCAGGGT	CTGGTGCTGTGGTCTTCTCAA
Nenf	GAAGGGAGTGGTGTTCGATGT	GTGTCGTGAGTGAGGTCTGC

Data was analyzed with CFX Manager software (BioRad) and Ct-values were averaged and normalized to the expression of *Hprt*, as this gene was found to be among the more stable reference genes for LPS-stimulated microglia. Data are expressed as relative mRNA levels with standard errors of the mean of duplicate reactions, which was calculated with the REST 2009 software.[56]

Enzyme-linked immunosorbent assay (ELISA)

ELISA was performed using an IL-6 Mouse uncoated ELISA KIT (Thermo Fisher, 88-7064-88) following the manufacturers protocol with minor modifications. In short, half-area high-binding 96 well plates (Greiner) were coated with 25 µL of coating antibody in PBS (1:250) overnight at 4 °C. The wells were blocked with 100 µL of diluent buffer for 2 h at rt. Incubation with 25 µL (diluted) supernatant and provided standard was done for 2 h at rt. The plates were then washed five times with PBS-T (PBS supplemented with 0.05% (w/v) Tween-20). 25 µL of the biotinylated detection antibody in diluent was incubated for 1 hour at rt, after which the plate was washed again five times with PBST. The secondary antibody in diluent was incubated 30 min at rt and the plate was washed seven times with PBST. Detection was done by reacting 25 µL of TMB solution in each well for 10-20 min before quenching with 12.5 µL of 1M aq. HCl. Absorption was measured at 450 nm using a CLARIOstar plate reader (BMG Labtech) and analyzed with Graphpad Prism 8.1.1.

DAN assay

To 100 µL of freshly isolated supernatant in a black 96-well plate was added 10 µL of 0.05 mg/mL 2,3-diethylaminonaphtalene (DAN) in 0.62 M aq. HCl. This was mixed and incubated for 30 min in the dark. The reaction was quenched with 10 µL of 1.4 M aq. NaOH. The solution was subsequently scanned for fluorescence at 365 nm excitation and 450 nm emission in a CLARIOstar plate reader (BMG Labtech). The concentration was determined using a standard curve of a freshly prepared dilution of $NaNO_2$ in medium.

Viability assay

Cells were seeded at $2.0x10^4$ or $3.0x10^4$ cells per well in a 96-well plate in 0.1 mL medium per well 24 h before treatment. The cells were then treated with the indicated stimuli in fresh complete medium. Afterwards, the culture medium was collected for DAN assay or ELISA. For the MTT assay, the medium was replaced with 90 µL fresh medium supplemented with 10 µL PBS with 5 mg/mL 3-(4,5-dimethylthiazol-2-yl)-2,5-diphenyltetrazolium (0.5 mg/mL final) and the plate was incubated at 37 °C for 3 h. The medium was removed and the formed formazan crystals were dissolved in 100 µL DMSO by shaking the plates at 800 rpm for 5 min. Absorbance was measured at 450 nm in a CLARIOstar plate reader (BMG Labtech) and data was analyzed using Graphpad Prism 8.1.1.

AfBPP of N9 microglia

Probe labeling and gel-based AfBPP

N9 microglia were grown to ~70% confluency on 6-well plates. They were washed with PBS (2 mL) and pac-DHA (**3**) or pac-DHEA (**4**) (10 µM from 10 mM ethanolic stock) was added in serum-free medium. The cells were incubated for 30 min at 37 °C after which the medium was aspirated and replaced with fresh medium and the cells were incubated for 4 or 24 h. Medium was aspirated, the cells were washed with PBS (1 mL) and ice-cold PBS (1 mL) was added. The cells were irradiated using a Caprobox™ (10 min, 4 °C, 350 nm, "UV") or exposed to ambient light (10 min, 4 °C, "No UV"). The PBS was collected in tubes and floating cells were spun down (1,000 *g*, 10 min, 4 °C) and the PBS aspirated. The cells in the wells were collected by scraping into ice-cold PBS (0.5 mL) and combined with the cell pellet. The cells were lysed with lysis buffer (250 µL, 250 mM sucrose, 1X protease inhibitor cocktail (Roche), 20 mM HEPES pH 7.5, 1 mM $MgCl_2$). This was sonicated (Branson Sonifier probe sonicator, 10 x 2 s pulses, 10% amplitude). Protein concentration was measured by Qubit™ assay (Invitrogen) and the samples were adjusted to 0.27 mg/mL and a volume of 440 µL, of which 40 µL was reserved for gel analysis. For gel analysis, 40 µL lysate was treated with freshly prepared click mix (4.37 µL per sample: 2.19 µL aq. 25 mM $CuSO_4$, 1.3 µL aq. 250 mM NaAsc, 0.44 µL 25 mM THPTA in DMSO, 0.44 µL 0.9 mM Cy5-N_3 in DMSO) and left at rt for 1 h in the dark. Samples were then quenched by addition of 4X Laemmli buffer, boiled (5 min, 95 °C) and resolved by SDS-PAGE (10% acrylamide gel, ±80 min, 180 V) along with protein marker (PageRuler™ Plus, Thermo Fisher). In-gel fluorescence was measured in the Cy3- and Cy5-channel (Chemidoc™ MP, Bio-Rad) and gels were stained with Coomassie after scanning.

Mass spectrometric analysis of tryptic peptides, identification and quantification

The pulldown experiment was performed as earlier described, with minor adjustments.[31,57] The lysates (400 µL) were subjected to a click reaction with freshly prepared click mix (43.7 µL per sample: 21.9 µL aq. 25 mM $CuSO_4$, 13 µL aq. 250 mM NaAsc, 4.4 µL 25 mM THPTA in DMSO, 4.4 µL 2.25 mM biotin-N_3 in DMSO) at rt for 1 h. Proteins were precipitated by addition of HEPES buffer (50 µL, 50 mM, pH 7.5), MeOH (666 µL), $CHCl_3$ (166 µL) and MilliQ (150 µL), vortexing after each addition. After spinning down (1,500 *g*, 10 min) the upper and lower layer were aspirated and the protein pellet was resuspended in MeOH (600 µL) by sonication (Branson Sonifier probe sonicator, 10 x 0.5 s pulses, 10% amplitude). The proteins were spun down (20,000 *g*, 5 min) and the MeOH was aspirated. The proteins were then redissolved in 6 M urea (500 µL) with 25 mM NH_4HCO_3 for 15 min, followed by reduction (65 °C, 15 min, 800 rpm shaking) with DTT (5 µL, 1 M). The samples were allowed to reach rt and proteins were alkylated (30 min) with IAA (40 µL, 0.5 M) in the dark. 140 µL SDS (10% w/v) was added and the samples were spun down (1,000 *g*, 5 min). They were transferred to 5 mL PBS containing 50 µL avidin agarose resin (Pierce, 100 µL of a 50% slurry, prewashed twice with 6 mL PBS + 0.5% SDS and once with 6 mL PBS) and incubated for 2 h while rotating. The beads were spun down (2,000 *g*, 2 min) and washed (3 x PBS + 0.5% SDS, 2 x PBS, 1 x MilliQ). The beads were resuspended in digestion buffer (250 µL, 100 mM Tris pH 7.8, 100 mM NaCl, 1 mM $CaCl_2$, 2% (v/v) acetonitrile, sequencing grade trypsin (Promega, 0.25 µg)) and transferred to low-binding tubes (Sarstedt) and incubated while shaking overnight (16 h, 37 °C, 1,000 rpm). Trypsin was quenched with 12.5 µL formic acid (LC-MS grade) and the beads were filtered off over a Bio-Spin column (BioRad, 400 *g*, 5 min), collecting the flow-through in a new 2 mL tube. Samples were added on C18 stagetips[58] (preconditioned with 50 µL MeOH, then 50 µL of 0.5% (v/v) formic acid in 80% (v/v) acetonitrile/MilliQ (solution B) and then 50 µL 0.5% (v/v) formic acid in MilliQ (solution A) by centrifugation (600 *g*, 2 min)). The peptides were washed with solution A (100 µL, 800 *g*, 3 min) and eluted into new low-binding tubes using solution B (100 µL, 800 *g*, 3 min). Samples were concentrated using an Eppendorf speedvac (Eppendorf Concentrator Plus 5301) and redissolved in LC-MS solution (30 µL per sample: 28.5 µL MilliQ, 2.85 µL acetonitrile, 0.095 µL formic acid, 600 fmol yeast enolase peptide digest (Waters, 186002325)). Samples were measured using a NanoACQUITY UPLC System coupled to a SYNAPT G2-Si high definition mass spectrometer (Waters). The peptides were separated using an analytical column (HSS-T3 C18 1.8 µm, 75 µm x 250 mm, Waters) with a concave gradient (5 to 40% acetonitrile in H_2O with 0.1% formic acid). [Glu^1]-fibrinopeptide B was used as lock mass. Mass spectra were acquired using the $UDMS^e$ method. The mass range was set from 50 to 2,000 Da with a scan time of 0.6 seconds in positive, resolution mode. The collision energy was set to 4 V in the trap cell for low-energy MS mode. For the elevated energy scan, the transfer cell collision energy was ramped using drift-time-specific collision energies. The lock mass is sampled every 30 seconds. For raw data processing, Progenesis QI for proteomics was used with the following parameters to search the murine proteome from Uniprot (Table S2).

Table S2 | Parameters used for Progenesis QI.

Parameter	Value
Lock mass *m*/*z* value	785.8426
Low energy threshold	150 counts
Elevated energy threshold	30 counts
Digest reagent	Trypsin
Missed cleavages	Max 2
Modifications	Fixed carbamidomethyl C, variable oxidation M
FDR less than	1%
Minimum fragments/peptide	2
Minimum fragments/protein	5
Minimum peptides/protein	1
Minimum peptide score for quantification	5.5
Identified ion charges for quantification	$2/3/4/5/6/7^+$

Transfection of HEK-293-T for gel-based AfBPP

HEK-293-T cells expressing hNENF, mNENF or mAPMAP were generated by seeding HEK-293-T cells on 12-wells plates ($4.0x10^4$ cells/cm^2) 24 h before transfection. Culture medium was aspirated and replaced with 400 µL fresh medium. A 3:1 (m/m) mixture of polyethylenimine (PEI) (1.875 µg/well) and plasmid DNA (0.625 µg/well) was prepared in serum-free culture medium (100 µL) and incubated for 15 min at rt. Transfection was performed by dropwise addition of the PEI/DNA mix to the cells. After 24 h, medium was refreshed. Cells were used 48 h post-transfection. Growth medium was aspirated and a solution of pac-DHEA (10 µM from a 10 mM stock) in serum-free DMEM supplemented with 0.1% (w/v) delipidated BSA (0.5 mL) was added and the cells were incubated for indicated time at 37 °C. Medium was aspirated and replaced with 1 mL ice-cold DPBS and the cells were irradiated using a Caprobox™ (10 min, 4 °C, 350 nm, "UV") or exposed to ambient light (10 min, 4 °C, "No UV"). The cells were harvested by pipetting and pelleted by centrifugation (1,000 *g*, 10 min, 4 °C). The supernatant was removed and the cells were lysed by resuspension in lysis buffer (250 mM sucrose, 20 mM HEPES pH 7.5, 1 mM $MgCl_2$, 1X protease inhibitor cocktail (Roche), 25 U/mL benzonase) and sonication in a bath sonicator (0 °C, 5 min). Protein concentration was measured by Qubit™ assay (Invitrogen) and the samples were adjusted to 1.5 mg/mL and a volume of 100 µL. For hNENF- and mNENF-transfected cells, 24 h post-transfection the medium was replaced with serum-free medium and after 24 h the supernatant was collected in tubes, spun down (1,000 *g*, 5 min) and concentrated on 10 kDa Amicon MW cutoff filters (Sigma) to 100 µL. The supernatant was then treated with pac-DHEA (10 µM from a 10 mM stock) for 30 min at rt and irradiated using a Caprobox™ (10 min, 4 °C, 350 nm).

All samples were treated with 10.4 µL click mix (5.5 µL aq. 25 mM $CuSO_4$, 3.25 µL aq. 250 mM NaAsc, 1.1 µL 25 mM THPTA in DMSO, 0.55 µL 0.9 mM Cy5-N_3 in DMSO) and left at r.t. for 1 h. Samples were then quenched by addition of 4X Laemmli buffer, boiled (5 min, 95 °C) and resolved by SDS-PAGE (10% acrylamide gel, ±80 min, 180 V) along with protein marker (PageRuler™ Plus, Thermo Fisher). In-gel fluorescence was measured in the Cy3- and Cy5-channel (Chemidoc™ MP, Bio-Rad) and the gels were subsequently stained with Coomassie and imaged as a loading control for normalization of fluorescence intensity. Alternatively, proteins were transferred to a 0.2 µm polyvinylidene difluoride membrane by Trans-Blot Turbo™ Transfer system (Bio-Rad). Membranes were washed with TBS (50 mM Tris pH 7.5, 150 mM NaCl) and blocked with 5% (w/v) milk in TBS-T (50 mM Tris pH 7.5, 150 mM NaCl, 0.05% (w/v) Tween-20) for 1 h at rt. Membranes were incubated with primary antibody mouse-anti-FLAG (F3156, Sigma Aldrich, 1:2,000, 1 h, rt) in the blocking solution. The membranes were then washed three times with TBS-T (5 min) and incubated with secondary goat-anti-mouse-HRP (sc-2005, Santa Cruz, 1:5,000 in 5% (w/v) milk in TBS-T, 1 h, rt) and washed three times with TBS-T and once with TBS. Membranes were developed in luminol development solution (10 mL of 1.4 mM luminol in 100 mM Tris pH 8.8 + 100 µL of 6.7 mM *p*-coumaric acid in DMSO + 3 µL of 30% (v/v) H_2O_2) and chemiluminescence was detected on ChemiDoc™ MP (Bio-Rad) in the chemiluminescence channel and colorimetric channel for the protein marker. Images were processed using Image Lab 6.0.1 (BioRad).

Western blot of N9 microglia

Expression of GSTM1-GFP and APMAP-GFP was checked by washing WT, GFP-, GSMT1-GFP- and APMAP-GFP-expressing cells with PBS and harvesting the cells in ice-cold PBS by scraping. Expression of endogenous GSMT1 and APMAP was checked by treatment of the cells with PBS or LPS (100 ng/mL) for 24 h, washing with PBS and harvesting the cells in ice-cold PBS by scraping. The cells were pelleted by centrifugation (1,000 *g*, 5 min) and lysed by resuspension in lysis buffer (250 mM sucrose, 20 mM HEPES pH 7.5, 1 mM $MgCl_2$, 1X protease inhibitor cocktail (Roche), 25 U/mL benzonase) and sonication in a bath sonicator (0 °C, 5 min). Protein concentration was measured by Qubit™ assay (Invitrogen) and the samples were adjusted to 1.5 mg/mL. Proteins were then denatured by adding 4X Laemmli buffer, boiled (5 min, 95 °C) and resolved by SDS-PAGE (10% acrylamide gel, ±80 min, 180 V) along with protein marker (PageRuler™ Plus, Thermo Fisher). Part of the gel was stained with Coomassie and imaged as a loading control. The rest of the gel was transferred to a 0.2 µm polyvinylidene difluoride membrane by Trans-Blot Turbo™ Transfer system (Bio-Rad). Membranes were washed with TBS (50

mM Tris pH 7.5, 150 mM NaCl) and blocked with 5% (w/v) milk in TBS-T (50 mM Tris pH 7.5, 150 mM NaCl, 0.05% (w/v) Tween-20) for 1 h at rt.

For endogenous protein, membranes were washed three times with TBS-T, followed by incubation with primary antibody in 5% (w/v) BSA in TBS-T (GSTM1, 13289748, 1:1,000, o/n, 4 °C or APMAP, 15985444, Fisher Scientific, 1:500, o/n, 4 °C). Membranes were then washed three times with TBS-T and incubated with matching secondary antibody in 5% (w/v) milk in TBS-T (1:5,000, 1 h at rt), then washed three times with TBS-T and once with TBS before developing.

For lentivirus-infected lysates, membranes were either directly incubated in the blocking solution with primary antibody (APMAP, 15985444, Fisher Scientific, 1:2,000, 1 h, rt) or washed three times with TBS-T, followed by incubation with primary antibody in 5% (w/v) BSA in TBS-T (GSTM1, 13289748, 1:1,000, 1 h, rt). Membranes were washed three times with TBS-T and incubated with matching secondary antibody in 5% (w/v) milk in TBS-T (1:4,000, 1 h at rt), then washed three times with TBS-T and once with TBS before developing.

Membranes were developed in luminol development solution (10 mL of 1.4 mM luminol in 100 mM Tris pH 8.8 + 100 µL of 6.7 mM *p*-coumaric acid in DMSO + 3 µL of 30% (v/v) H_2O_2) and chemiluminescence was detected on ChemiDoc™ MP (Bio-Rad) in the chemiluminescence channel and colorimetric channel for the protein marker. Images were processed using Image Lab 6.0.1 (BioRad). Secondary antibodies: goat anti-mouse-HRP (Santa Cruz, sc-2005), goat anti-rabbit-HRP (Santa Cruz, sc-2030).

Confocal microscopy

Cells were grown on an ibidi 8 well µ-Slide (1.5 polymer coverslip, ibiTreat) and mounted in a Okolab cage incubator warmed to 37 °C, supplied with 5% CO_2. For live cell microscopy, RPMI containing 2 mM GlutaMAX, 100 I.U./mL penicillin and 50 µg/mL streptomycin was used during image acquisition. For fixed samples, mounting medium of 9:1 glycerol:PBS containing 1% DABCO anti-bleaching agent was used. All images were collected using an Andor DragonFly 505 spinning disk confocal system, containing an 8-line integrated laser engine, on a Leica DMi8 inverted microscope equipped with a 63X/1.40-0.60 HCX PL APO oil objective. Hoechst 33342 was excited with the 405 line and collected with the 450/50 BP emission filter. GFP-fusion proteins were excited with the 488 line and collected with the 525/50 BP emission filter. Images were acquired with the Zyla 2048x2048 sCMOS camera and 2x2 camera binning controlled with the integrated Fusion software. Z-series optical sections were collected with a system-optimized step-size of 0.13 microns and deconvolved using the integrated ClearView-GPU™ deconvolution software. Z-series are displayed as maximum z-projections, and gamma, brightness and contrast were adjusted using FIJI.[59]

Statistical analysis

Unless otherwise noted, all replicates represent biological replicates and all data represent means ± SEM. Statistical significance between two conditions was determined using Student's t-tests (two-tailed, unpaired). Statistical significance between multiple conditions was tested using a one-way ANOVA with Dunnett's multiple comparisons correction, or when all conditions were compared, Tukey's multiple comparisons correction. *** $p < 0.001$; ** $p < 0.01$; * $p < 0.05$; n.s. if $p > 0.05$. All statistical analysis was conducted using Graphpad Prism 8.1.1 or Microsoft Excel.

Synthesis

General remarks

Dry DCM was prepared by storage on activated 4 Å molecular sieves for at least 24 hours. All reagents were purchased from Alfa Aesar, Sigma Aldrich/Merck or Acros and used without further purification. Flash column chromatography was performed using SiliCycle silica gel type SiliaFlash P60 (230-400 mesh). TLC analysis was performed on Merck silica gel 60/Kieselguhr F254, 0.25 mm. Compounds were visualized using $KMnO_4$ stain (K_2CO_3 (40 g), $KMnO_4$ (6 g), and water (600 mL)). ^1H NMR and ^{13}C NMR spectra were recorded on a Bruker AV-400 (400 MHz) spectrometer. Chemical shift values are reported in ppm relative to the tetramethylsilane signal for ^1H NMR (δ = 0 ppm) and relative to the solvent signal of $CDCl_3$ for ^{13}C NMR (δ = 77.16 ppm). Data are reported as follows: Chemical shifts (δ), multiplicity (s = singlet, d = doublet, dd = doublet of doublets, ddt = doublet of doublet of triplets, td = triplet of doublets, t = triplet, q = quartet, p = pentet, bs = broad singlet, m = multiplet), coupling constants *J* (Hz), and integration. High resolution mass spectra (HRMS) were recorded by direct injection on a q-TOF mass spectrometer (Synapt G2-SI) equipped with an electrospray ion source in positive mode with Leu-enkephalin (m/z = 556.2771) as an internal lock mass. The instrument was calibrated prior to measurement using the MS/MS spectrum of [Glu^1]-fibrinopeptide B.

(4*Z*,7*Z*,10*Z*,13*Z*,16*Z*,19*Z*)-21-(3-(but-3-yn-1-yl)-3*H*-diazirin-3-yl)-*N*-(2-hydroxyethyl)henicosa-4,7,10,13,16,19-hexaenamide (pac-DHEA, 4)

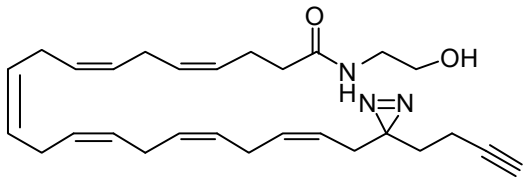

4*Z*,7*Z*,10*Z*,13*Z*,16*Z*,19*Z*)-21-(3-(but-3-yn-1-yl)-3*H*-diazirin-3-yl)henicosa-4,7,10,13,16,19-hexaenoic acid (0.0154 g, 0.038 mmol) (**3**, Chapter 3) was dissolved in dry DCM (1 mL) after which NHS (6.54 mg, 0.057 mmol), DIPEA (0.099 mL, 0.057 mmol) and EDC (0.0109 g, 0.057 mmol) were added and the reaction was stirred overnight. The reaction was poured into brine (5 mL) and the aq. layer was extracted with DCM (3 x 5 mL). The combined organic layers were dried over Na_2SO_4, filtered over a plug of silica and concentrated under reduced pressure. It was redissolved in dry DCM (1 mL) and DIPEA (0.033 mL, 0.189 mmol) was added, the mixture was cooled to 0 °C and ethanolamine (1 M in DCM, 0.189 mL, 0.189 mmol) was added dropwise. The reaction was allowed to reach rt and stirred for 1 h, after which it was concentrated under reduced pressure and purified by column chromatography twice (EtOAc/pentane = 1:1 to EtOAc, then MeOH/DCM = 1:128 to 1:65) to afford the title compound as a slightly yellow oil (0.0104 g, 0.023 mmol, 61%). R_f = 0.35 (EtOAc); ^1H NMR (400 MHz, $CDCl_3$) δ 5.99 (s, 1H), 5.53 (dtt, *J* = 10.7, 7.3, 1.7 Hz, 1H), 5.48 – 5.29 (m, 10H), 5.29 – 5.20 (m, 1H), 3.78 – 3.68 (m, 2H), 3.43 (q, *J* = 5.1 Hz, 2H), 2.84 (q, *J* = 6.5, 6.0 Hz, 8H), 2.75 (t, *J* = 7.1 Hz, 2H), 2.42 (p, *J* = 7.6 Hz, 4H), 2.28 (t, *J* = 7.4 Hz, 2H), 2.17 (dd, *J* = 7.6, 1.6 Hz, 2H), 2.06 – 1.95 (m, 3H), 1.65 (t, *J* = 7.3 Hz, 2H); ^{13}C NMR (101 MHz, $CDCl_3$) δ 173.87, 132.05, 129.66, 128.73, 128.45, 128.42, 128.32, 128.30, 128.17, 127.55, 121.94, 82.91, 69.30, 62.68, 42.69, 36.42, 32.10, 31.27, 28.32, 25.87, 25.80, 25.75, 23.54, 13.47; HRMS: Calculated for $[C_{28}H_{39}N_3O_2+H]^+$ 450.3115, found 450.3114.

Supplementary data

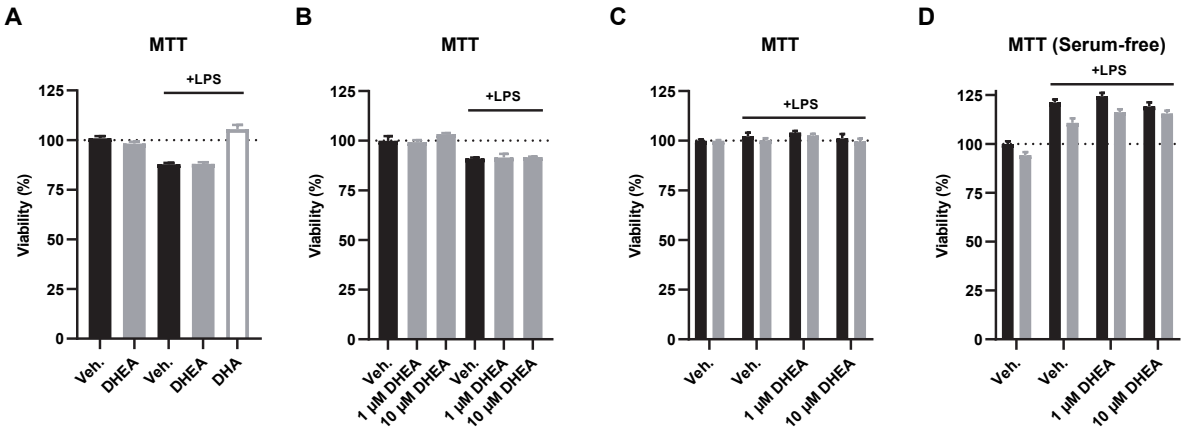

Figure S1 | Viability assay of N9 microglia corresponding to Figure 6A/B/C/D. The supernatant of treated N9 microglia was collected for DAN assay or IL-6 ELISA and viability was tested by MTT assay. Data represent means ± SEM (n = 3-6).

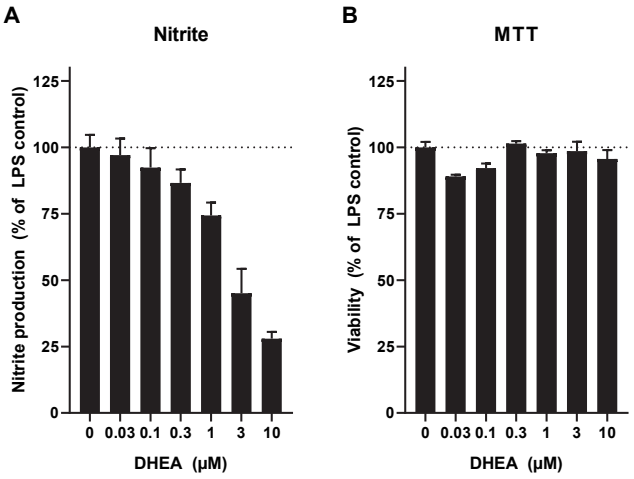

Figure S2 | DHEA dose-dependently decreases NO production of N9 microglia after LPS stimulation. N9 microglia were pretreated with DHEA or vehicle for 4 h before LPS stimulation (100 ng/mL) for 24 h. Supernatant was collected for **(A)** DAN assay and viability was tested by **(B)** MTT assay. Data represent means ± SEM (n = 3).

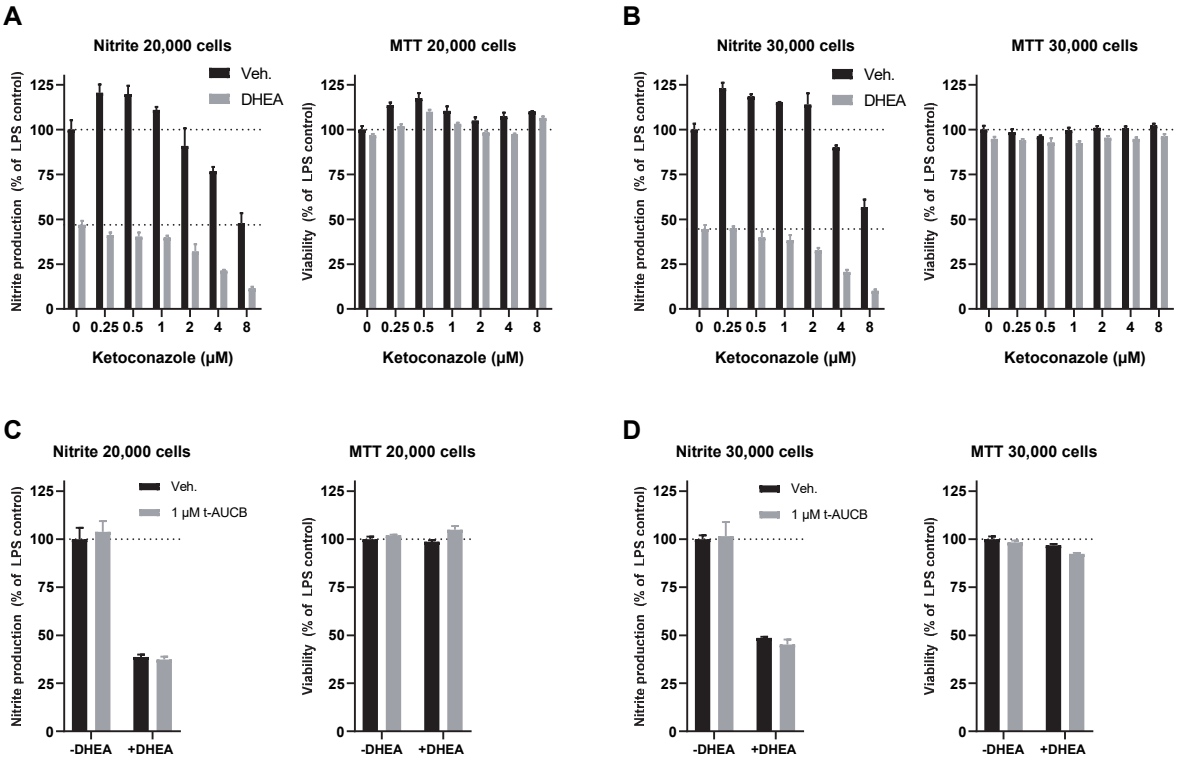

Figure S3 | Ketoconazole or t-AUCB do not influence the anti-inflammatory effects of DHEA. (A, C) 20,000 or **(B, D)** 30,000 N9 microglia were pretreated with indicated combination of ketoconazole, t-AUCB, 10 μM DHEA or vehicle for 4 h before LPS stimulation (100 ng/mL) for 24 h. Supernatant was collected for DAN assay and viability was tested by MTT assay. Data represent means ± SEM (n = 3).

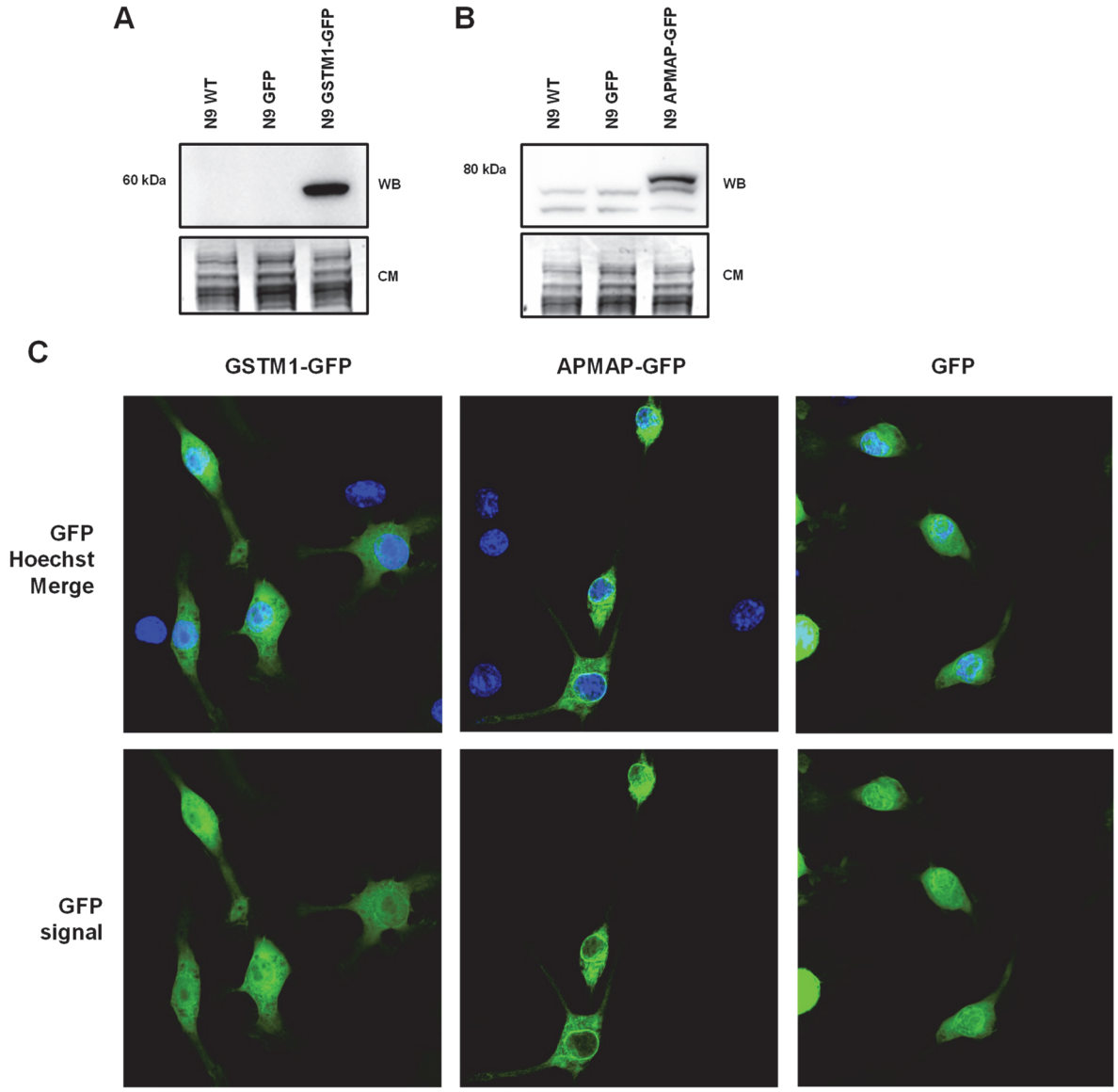

Figure S4 | Expression of GFP, GSTM1-GFP and APMAP-GFP in N9 microglia. (A) GSMT1 and **(B)** APMAP western blot of N9 microglia lysate confirms expression of the GFP fusion proteins. Coomassie served as loading control. **(C)** Live-cell confocal microscopy shows GSMT1-GFP is homogeneously localized in the cell whereas APMAP-GFP is excluded from the nucleus in N9 microglia.

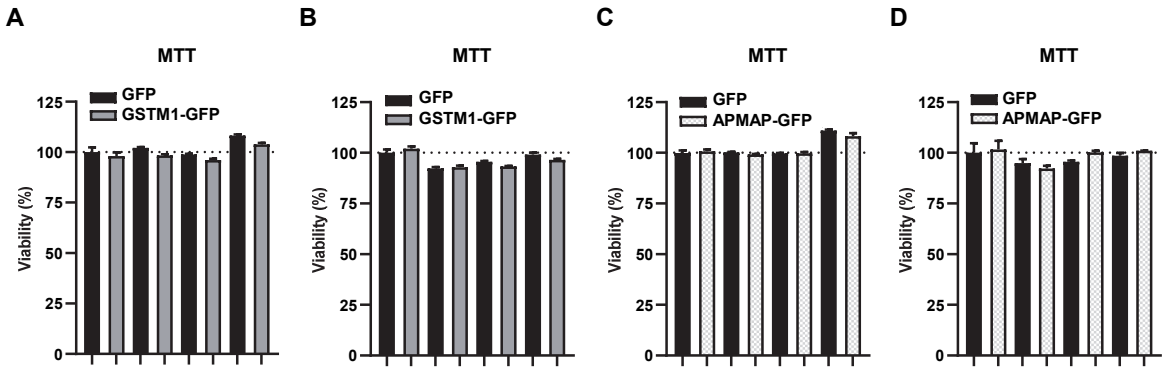

Figure S5 | Viability assay of N9 microglia corresponding to Figure 7A/B/C/D. The supernatant of treated N9 microglia was collected for DAN assay or IL-6 ELISA and viability was tested by MTT assay. Data represent means ± SEM (n = 4).

Table S3 | Proteins significantly and specifically UV-enriched by pac-DHEA (4) in N9 microglia.

Gene name	Unique peptides	Description	UV/no UV pac-DHEA (4)	p-value	UV/UV pac-DHEA (4) vs pac-DHA (3), 24h	p-value	UV/UV pac-DHEA (4) vs pac-DHA (3), 4h
APMAP	**11**	**Adipocyte plasma membrane-associated protein**	**47.47**	**0.0319**	**21.27**	**0.0334**	**4.85**
PMPCA	7	Mitochondrial-processing peptidase subunit alpha	7.78	0.0405	7.92	0.0408	6.67
NUCB1	8	Nucleobindin-1	5.57	0.0064	6.48	0.0040	5.17
NENF	**6**	**Neudesin**	**69.34**	**0.0094**	**6.43**	**0.0128**	**2.69**
GSTM1	**4**	**Glutathione S-transferase Mu 1**	**5.88**	**0.0216**	**3.70**	**0.0321**	**2.83**
PTGR2	7	Prostaglandin reductase 2	22.54	0.0132	3.19	0.0248	2.83
ACP6	5	Lysophosphatidic acid phosphatase type 6	5.35	0.0022	3.07	0.0100	1.82
HMOX2	11	Heme oxygenase 2	2.53	0.0069	2.68	0.0014	2.17
MTAP	12	S-methyl-5'-thioadenosine phosphorylase	6.70	0.0214	2.45	0.0260	10.20
ALDH2	19	Aldehyde dehydrogenase 2	4.48	0.0077	2.33	0.0372	1.40
UGT1A7C	11	UDP-glucuronosyltransferase 1-7C	3.43	0.0017	2.30	0.0008	0.87

References

(1) Salem, N.; Litman, B.; Kim, H.-Y.; Gawrisch, K. Mechanisms of Action of Docosahexaenoic Acid in the Nervous System. *Lipids* **2001**, *36* (9), 945–959.

(2) Kawakita, E.; Hashimoto, M.; Shido, O. Docosahexaenoic Acid Promotes Neurogenesis in Vitro and in Vivo. *Neuroscience* **2006**, *139* (3), 991–997.

(3) Calderon, F.; Kim, H.-Y. Docosahexaenoic Acid Promotes Neurite Growth in Hippocampal Neurons. *J. Neurochem.* **2004**, *90* (4), 979–988.

(4) Guemez-Gamboa, A.; Nguyen, L. N.; Yang, H.; Zaki, M. S.; Kara, M.; Ben-Omran, T.; Akizu, N.; Rosti, R. O.; Rosti, B.; Scott, E.; Schroth, J.; Copeland, B.; Vaux, K. K.; Cazenave-Gassiot, A.; Quek, D. Q. Y.; Wong, B. H.; Tan, B. C.; Wenk, M. R.; Gunel, M.; Gabriel, S.; Chi, N. C.; Silver, D. L.; Gleeson, J. G. Inactivating Mutations in MFSD2A , Required for Omega-3 Fatty Acid Transport in Brain, Cause a Lethal Microcephaly Syndrome. *Nat. Genet.* **2015**, *47* (7), 809–813.

(5) Hsieh, A. T.; Anthony, J. C.; Diersen-Schade, D. A.; Rumsey, S. C.; Lawrence, P.; Li, C.; Nathanielsz, P. W.; Brenna, J. T. The Influence of Moderate and High Dietary Long Chain Polyunsaturated Fatty Acids (LCPUFA) on Baboon Neonate Tissue Fatty Acids. *Pediatr. Res.* **2007**, *61* (5), 537–545.

(6) Park, T.; Chen, H.; Kevala, K.; Lee, J.-W.; Kim, H.-Y. N-Docosahexaenoylethanolamine Ameliorates LPS-Induced Neuroinflammation via CAMP/PKA-Dependent Signaling. *J. Neuroinflammation* **2016**, *13* (1), 284.

(7) Rashid, M. A.; Kim, H.-Y. N-Docosahexaenoylethanolamine Ameliorates Ethanol-Induced Impairment of Neural Stem Cell Neurogenic Differentiation. *Neuropharmacology* **2016**, *102*, 174–185.

(8) Kim, H.-Y.; Moon, H.-S.; Cao, D.; Lee, J.; Kevala, K.; Jun, S. B.; Lovinger, D. M.; Akbar, M.; Huang, B. X. N-Docosahexaenoylethanolamide Promotes Development of Hippocampal Neurons. *Biochem. J.* **2011**, *435* (2), 327–336.

(9) Kharebava, G.; Rashid, M. A.; Lee, J.-W.; Sarkar, S.; Kevala, K.; Kim, H.-Y. N-Docosahexaenoylethanolamine Regulates Hedgehog Signaling and Promotes Growth of Cortical Axons. *Biol. Open* **2015**, *4* (12), 1660–1670.

(10) Watson, J. E.; Kim, J. S.; Das, A. Emerging Class of Omega-3 Fatty Acid Endocannabinoids & Their Derivatives. *Prostaglandins Other Lipid Mediat.* **2019**, *143*, 106337.

(11) Meijerink, J.; Plastina, P.; Vincken, J.-P.; Poland, M.; Attya, M.; Balvers, M.; Gruppen, H.; Gabriele, B.; Witkamp, R. F. The Ethanolamide Metabolite of DHA, Docosahexaenoylethanolamine, Shows Immunomodulating Effects in Mouse Peritoneal and RAW264.7 Macrophages: Evidence for a New Link between Fish Oil and Inflammation. *Br. J. Nutr.* **2011**, *105* (12), 1798–1807.

(12) Heneka, M. T.; Kummer, M. P.; Latz, E. Innate Immune Activation in Neurodegenerative Disease. *Nat. Rev. Immunol.* **2014**, *14* (7), 463–477.

(13) Lull, M. E.; Block, M. L. Microglial Activation and Chronic Neurodegeneration. *Neurotherapeutics* **2010**, *7* (4), 354–365.

(14) Morales, I.; Guzmán-Martínez, L.; Cerda-Troncoso, C.; Farías, G. A.; Maccioni, R. B. Neuroinflammation in the Pathogenesis of Alzheimer's Disease. A Rational Framework for the Search of Novel Therapeutic Approaches. *Front. Cell. Neurosci.* **2014**, *8*.

(15) Lawson, L. J.; Perry, V. H.; Dri, P.; Gordon, S. Heterogeneity in the Distribution and Morphology of Microglia in the Normal Adult Mouse Brain. *Neuroscience* **1990**, *39* (1), 151–170.

(16) Cherry, J. D.; Olschowka, J. A.; O'Banion, M. K. Neuroinflammation and M2 Microglia: The Good, the Bad, and the Inflamed. *J. Neuroinflammation* **2014**, *11* (1), 98.

(17) Leyrolle, Q.; Layé, S.; Nadjar, A. Direct and Indirect Effects of Lipids on Microglia Function. *Neurosci. Lett.* **2019**, *708*, 134348.

(18) Ekdahl, C. T. Microglial Activation – Tuning and Pruning Adult Neurogenesis. *Front. Pharmacol.* **2012**, *3*.

(19) Park, T.; Chen, H.; Kim, H.-Y. GPR110 (ADGRF1) Mediates Anti-Inflammatory Effects of N-Docosahexaenoylethanolamine. *J. Neuroinflammation* **2019**, *16* (1), 225.

(20) Meijerink, J.; Poland, M.; Balvers, M. G. J.; Plastina, P.; Lute, C.; Dwarkasing, J.; van Norren, K.; Witkamp, R. F. Inhibition of COX-2-Mediated Eicosanoid Production Plays a Major Role in the Anti-Inflammatory Effects of the Endocannabinoid N-Docosahexaenoylethanolamine (DHEA) in Macrophages. *Br. J. Pharmacol.* **2015**, *172* (1), 24–37.

(21) Bus, I. de; Zuilhof, H.; Witkamp, R.; Balvers, M.; Albada, B. Novel COX-2 Products of n-3 Polyunsaturated Fatty Acid-Ethanolamine-Conjugates Identified in RAW264.7 Macrophages. *J. Lipid Res.* **2019**, *60* (11), 1829–1840.

(22) McDougle, D. R.; Watson, J. E.; Abdeen, A. A.; Adili, R.; Caputo, M. P.; Krapf, J. E.; Johnson, R. W.; Kilian, K. A.; Holinstat, M.; Das, A. Anti-Inflammatory ω-3 Endocannabinoid Epoxides. *Proc. Natl. Acad. Sci.* **2017**, *114* (30), E6034–E6043.

(23) Spector, A. A.; Fang, X.; Snyder, G. D.; Weintraub, N. L. Epoxyeicosatrienoic Acids (EETs): Metabolism and Biochemical Function. *Prog. Lipid Res.* **2004**, *43* (1), 55–90.

(24) Deng, Y.; Theken, K. N.; Lee, C. R. Cytochrome P450 Epoxygenases, Soluble Epoxide Hydrolase, and the Regulation of Cardiovascular Inflammation. *J. Mol. Cell. Cardiol.* **2010**, *48* (2), 331–341.

(25) Yang, R.; Fredman, G.; Krishnamoorthy, S.; Agrawal, N.; Irimia, D.; Piomelli, D.; Serhan, C. N. Decoding Functional Metabolomics with Docosahexaenoyl Ethanolamide (DHEA) Identifies Novel Bioactive Signals. *J. Biol. Chem.* **2011**, *286* (36), 31532–31541.
(26) Alhouayek, M.; Bottemanne, P.; Makriyannis, A.; Muccioli, G. G. N-Acylethanolamine-Hydrolyzing Acid Amidase and Fatty Acid Amide Hydrolase Inhibition Differentially Affect N-Acylethanolamine Levels and Macrophage Activation. *Biochim. Biophys. Acta BBA - Mol. Cell Biol. Lipids* **2017**, *1862* (5), 474–484.
(27) Lapinsky, D. J.; Johnson, D. S. Recent Developments and Applications of Clickable Photoprobes in Medicinal Chemistry and Chemical Biology. *Future Med. Chem.* **2015**, *7* (16), 2143–2171.
(28) Hein, J. E.; Fokin, V. V. Copper-Catalyzed Azide–Alkyne Cycloaddition (CuAAC) and beyond: New Reactivity of Copper(I) Acetylides. *Chem. Soc. Rev.* **2010**, *39* (4), 1302–1315.
(29) Stansley, B.; Post, J.; Hensley, K. A Comparative Review of Cell Culture Systems for the Study of Microglial Biology in Alzheimer's Disease. *J. Neuroinflammation* **2012**, *9*, 115.
(30) Weldon, S. M.; Mullen, A. C.; Loscher, C. E.; Hurley, L. A.; Roche, H. M. Docosahexaenoic Acid Induces an Anti-Inflammatory Profile in Lipopolysaccharide-Stimulated Human THP-1 Macrophages More Effectively than Eicosapentaenoic Acid. *J. Nutr. Biochem.* **2007**, *18* (4), 250–258.
(31) van Rooden, E. J.; Florea, B. I.; Deng, H.; Baggelaar, M. P.; van Esbroeck, A. C. M.; Zhou, J.; Overkleeft, H. S.; van der Stelt, M. Mapping *in Vivo* Target Interaction Profiles of Covalent Inhibitors Using Chemical Proteomics with Label-Free Quantification. *Nat. Protoc.* **2018**, *13* (4), 752–767.
(32) Huang, D. W.; Sherman, B. T.; Lempicki, R. A. Systematic and Integrative Analysis of Large Gene Lists Using DAVID Bioinformatics Resources. *Nat. Protoc.* **2009**, *4* (1), 44–57.
(33) Huang, D. W.; Sherman, B. T.; Lempicki, R. A. Bioinformatics Enrichment Tools: Paths toward the Comprehensive Functional Analysis of Large Gene Lists. *Nucleic Acids Res.* **2009**, *37* (1), 1–13.
(34) Niphakis, M. J.; Lum, K. M.; Cognetta III, A. B.; Correia, B. E.; Ichu, T.-A.; Olucha, J.; Brown, S. J.; Kundu, S.; Piscitelli, F.; Rosen, H.; Cravatt, B. F. A Global Map of Lipid-Binding Proteins and Their Ligandability in Cells. *Cell* **2015**, *161* (7), 1668–1680.
(35) Kano, S.; Choi, E. Y.; Dohi, E.; Agarwal, S.; Chang, D. J.; Wilson, A. M.; Lo, B. D.; Rose, I. V. L.; Gonzalez, S.; Imai, T.; Sawa, A. Glutathione S-Transferases Promote Proinflammatory Astrocyte-Microglia Communication during Brain Inflammation. *Sci Signal* **2019**, *12* (569), eaar2124.
(36) Ignarro, L. J.; Fukuto, J. M.; Griscavage, J. M.; Rogers, N. E.; Byrns, R. E. Oxidation of Nitric Oxide in Aqueous Solution to Nitrite but Not Nitrate: Comparison with Enzymatically Formed Nitric Oxide from L-Arginine. *Proc. Natl. Acad. Sci.* **1993**, *90* (17), 8103–8107.
(37) Bryan, N. S.; Grisham, M. B. Methods to Detect Nitric Oxide and Its Metabolites in Biological Samples. *Free Radic. Biol. Med.* **2007**, *43* (5), 645–657.
(38) Luo, Y.; Zheng, S. G. Hall of Fame among Pro-Inflammatory Cytokines: Interleukin-6 Gene and Its Transcriptional Regulation Mechanisms. *Front. Immunol.* **2016**, *7*.
(39) Kimura, I.; Nakayama, Y.; Zhao, Y.; Konishi, M.; Itoh, N. Neurotrophic Effects of Neudesin in the Central Nervous System. *Front. Neurosci.* **2013**, *7*.
(40) Burke, B.; Sumner, S.; Maitland, N.; Lewis, C. E. Macrophages in Gene Therapy: Cellular Delivery Vehicles and in Vivo Targets. *J. Leukoc. Biol.* **2002**, *72* (3), 417–428.
(41) Carrillo-Jimenez, A.; Puigdellívol, M.; Vilalta, A.; Venero, J. L.; Brown, G. C.; StGeorge-Hyslop, P.; Burguillos, M. A. Effective Knockdown of Gene Expression in Primary Microglia With SiRNA and Magnetic Nanoparticles Without Cell Death or Inflammation. *Front. Cell. Neurosci.* **2018**, *12*.
(42) Ilhan, A.; Gartner, W.; Nabokikh, A.; Daneva, T.; Majdic, O.; Cohen, G.; Böhmig, G. A.; Base, W.; Hörl, W. H.; Wagner, L. Localization and Characterization of the Novel Protein Encoded by C20orf3. *Biochem. J.* **2008**, *414* (3), 485–495.
(43) Hulce, J. J.; Cognetta, A. B.; Niphakis, M. J.; Tully, S. E.; Cravatt, B. F. Proteome-Wide Mapping of Cholesterol-Interacting Proteins in Mammalian Cells. *Nat. Methods* **2013**, *10* (3), 259–264.
(44) Haberkant, P.; Stein, F.; Höglinger, D.; Gerl, M. J.; Brügger, B.; Van Veldhoven, P. P.; Krijgsveld, J.; Gavin, A.-C.; Schultz, C. Bifunctional Sphingosine for Cell-Based Analysis of Protein-Sphingolipid Interactions. *ACS Chem. Biol.* **2016**, *11* (1), 222–230.
(45) Bockelmann, S.; Mina, J. G. M.; Korneev, S.; Hassan, D. G.; Müller, D.; Hilderink, A.; Vlieg, H. C.; Raijmakers, R.; Heck, A. J. R.; Haberkant, P.; Holthuis, J. C. M. A Search for Ceramide Binding Proteins Using Bifunctional Lipid Analogs Yields CERT-Related Protein StarD7. *J. Lipid Res.* **2018**, *59* (3), 515–530.
(46) Kimura, I.; Nakayama, Y.; Yamauchi, H.; Konishi, M.; Miyake, A.; Mori, M.; Ohta, M.; Itoh, N.; Fujimoto, M. Neurotrophic Activity of Neudesin, a Novel Extracellular Heme-Binding Protein, Is Dependent on the Binding of Heme to Its Cytochrome B5-like Heme/Steroid-Binding Domain. *J. Biol. Chem.* **2008**, *283* (7), 4323–4331.
(47) Kimura, I.; Yoshioka, M.; Konishi, M.; Miyake, A.; Itoh, N. Neudesin, a Novel Secreted Protein with a Unique Primary Structure and Neurotrophic Activity. *J. Neurosci. Res.* **2005**, *79* (3), 287–294.
(48) Kimura, I.; Konishi, M.; Miyake, A.; Fujimoto, M.; Itoh, N. Neudesin, a Secreted Factor, Promotes Neural Cell Proliferation and Neuronal Differentiation in Mouse Neural Precursor Cells. *J. Neurosci. Res.* **2006**, *83* (8), 1415–1424.

(49) Ohta, H.; Konishi, M.; Kobayashi, Y.; Kashio, A.; Mochiyama, T.; Matsumura, S.; Inoue, K.; Fushiki, T.; Nakao, K.; Kimura, I.; Itoh, N. Deletion of the Neurotrophic Factor Neudesin Prevents Diet-Induced Obesity by Increased Sympathetic Activity. *Sci. Rep.* **2015**, *5* (1), 1–12.
(50) Mannervik, B. The Isoenzymes of Glutathione Transferase. In *Advances in Enzymology and Related Areas of Molecular Biology*; John Wiley & Sons, Ltd, 2006; pp 357–417.
(51) Wu, W.; Peden, D.; Diaz-Sanchez, D. Role of GSTM1 in Resistance to Lung Inflammation. *Free Radic. Biol. Med.* **2012**, *53* (4), 721–729.
(52) Cotton, S. C.; Sharp, L.; Little, J.; Brockton, N. Glutathione S-Transferase Polymorphisms and Colorectal Cancer: A HuGE Review. *Am. J. Epidemiol.* **2000**, *151* (1), 7–32.
(53) Saitou, M.; Satta, Y.; Gokcumen, O.; Ishida, T. Complex Evolution of the GSTM Gene Family Involves Sharing of GSTM1 Deletion Polymorphism in Humans and Chimpanzees. *BMC Genomics* **2018**, *19* (1), 293.
(54) Albrektsen, T.; Richter, H. E.; Clausen, J. T.; Fleckner, J. Identification of a Novel Integral Plasma Membrane Protein Induced during Adipocyte Differentiation. *Biochem. J.* **2001**, *359* (2), 393–402.
(55) Baggelaar, M. P.; Janssen, F. J.; van Esbroeck, A. C. M.; den Dulk, H.; Allarà, M.; Hoogendoorn, S.; McGuire, R.; Florea, B. I.; Meeuwenoord, N.; van den Elst, H.; van der Marel, G. A.; Brouwer, J.; Di Marzo, V.; Overkleeft, H. S.; van der Stelt, M. Development of an Activity-Based Probe and In Silico Design Reveal Highly Selective Inhibitors for Diacylglycerol Lipase-α in Brain. *Angew. Chem. Int. Ed.* **2013**, *52* (46), 12081–12085.
(56) Pfaffl, M. W.; Horgan, G. W.; Dempfle, L. Relative Expression Software Tool (REST©) for Group-Wise Comparison and Statistical Analysis of Relative Expression Results in Real-Time PCR. *Nucleic Acids Res.* **2002**, *30* (9), e36–e36.
(57) Soethoudt, M.; Stolze, S. C.; Westphal, M. V.; van Stralen, L.; Martella, A.; van Rooden, E. J.; Guba, W.; Varga, Z. V.; Deng, H.; van Kasteren, S. I.; Grether, U.; IJzerman, A. P.; Pacher, P.; Carreira, E. M.; Overkleeft, H. S.; Ioan-Facsinay, A.; Heitman, L. H.; van der Stelt, M. Selective Photoaffinity Probe That Enables Assessment of Cannabinoid CB2 Receptor Expression and Ligand Engagement in Human Cells. *J. Am. Chem. Soc.* **2018**, *140* (19), 6067–6075.
(58) Rappsilber, J.; Mann, M.; Ishihama, Y. Protocol for Micro-Purification, Enrichment, Pre-Fractionation and Storage of Peptides for Proteomics Using StageTips. *Nat. Protoc.* **2007**, *2* (8), 1896–1906.
(59) Schindelin, J.; Arganda-Carreras, I.; Frise, E.; Kaynig, V.; Longair, M.; Pietzsch, T.; Preibisch, S.; Rueden, C.; Saalfeld, S.; Schmid, B.; Tinevez, J.-Y.; White, D. J.; Hartenstein, V.; Eliceiri, K.; Tomancak, P.; Cardona, A. Fiji: An Open-Source Platform for Biological-Image Analysis. *Nat. Methods* **2012**, *9* (7), 676–682.